OPEN ACCESS

Applied Physics Express 11, 015501 (2018)

https://doi.org/10.7567/APEX.11.015501

Sublattice reversal in GaAs/Ge/GaAs heterostructures grown on (113)B GaAs substrates

Xiangmeng Lu[1]*, Naoto Kumagai[2], Yasuo Minami[1], and Takahiro Kitada[1]

[1]*Graduate School of Technology, Industrial and Social Sciences, Tokushima University, Tokushima 770-8506, Japan*
[2]*National Institute of Advanced Industrial Science and Technology (AIST), Nagoya 464-8601, Japan*

*E-mail: xm-lu@tokushima-u.ac.jp

Received October 6, 2017; accepted November 10, 2017; published online November 30, 2017

GaAs/Ge/GaAs heterostructures were grown on high-index (113)B GaAs substrates by molecular beam epitaxy. Sublattice reversal in GaAs/Ge/GaAs was identified by comparing the anisotropic etching profile of the epitaxial sample with that for reference (113)A and (113)B GaAs substrates. The shape of the resulting mesa for the lower GaAs layer was similar to that for the reference (113)B GaAs substrate, whereas that for the upper GaAs layer was similar to that for the reference (113)A GaAs substrate. An atomic-resolution analysis was also conducted by mapping using energy-dispersive X-ray spectroscopy, whereby the sublattice reversal was directly observed through the atomic arrangements.

Room-temperature terahertz (THz) light sources are highly desirable because of their wide range of potential applications, including wireless communications, spectroscopy, and imaging.[1,2] Several semiconductor-based devices, such as quantum cascade lasers (QCLs),[3–5] resonant tunneling diodes (RTDs),[6,7] and photomixers[8,9] have been studied and developed for use as continuous-wave THz emitters. Terahertz sources based on intracavity difference-frequency generation (DFG) in dual-wavelength mid-infrared QCLs have also been recently reported.[10,11] However, there are challenges associated with each of these devices. For example, the emission power of RTDs becomes insufficient when the devices are operated at higher frequencies. In addition, although significant progress has been made with regard to THz QCLs, near-room temperature operation has not been demonstrated.

Optical microcavities are good candidates for nonlinear optical devices because an extremely strong electric field is realized in the cavity layer sandwiched between two distributed Bragg reflector (DBR) multilayers. Efficient wavelength conversion is possible in a GaAs-based multilayer cavity when the structure is grown on a non-(001) substrate to take advantage of the second-order nonlinearity of zincblende-type semiconductors.[12] We have proposed a GaAs/AlAs coupled multilayer cavity structure for novel THz emitting devices.[13] The structure consists of two equivalent cavity layers and three DBR multilayers. Two cavity modes appear in the center of the high reflection band because a degenerate cavity mode is split into two different modes as a result of coupling of the cavity layers. The mode frequency difference can be precisely defined within the THz region in accordance with the number of pairs of intermediate DBRs. We have obtained a strong sum-frequency generation (SFG) signal from a GaAs/AlAs coupled multilayer cavity grown on a (113)B GaAs substrate when the two modes were simultaneously excited by 100 fs laser pulses.[14–16] DFG signals from the (113)B coupled cavity samples were also demonstrated at room temperature by time-resolved waveform measurements using 100 fs laser pulses and a photoconductive antenna.[17–19] From the viewpoint of practical device applications, the two modes should be generated inside the structure by current injection,[20–23] since this enables THz emission through DFG without external light sources.

The second-order nonlinear polarization of DFG from two cavity modes is given by $\chi^{(2)}E^*(\lambda_1)E(\lambda_2)$, where $\chi^{(2)}$ is the second-order nonlinear susceptibility, and $E(\lambda_1)$ and $E(\lambda_2)$ are the electric fields of the two modes inside the coupled multilayer cavity. Opposite signs of $\chi^{(2)}$ in the two cavity regions are necessary in order to realize stronger THz-DFG for the two modes. The sign of $\chi^{(2)}$ can be inverted by introducing 180° rotation of the crystal around the appropriate axis. Recently, we have successfully enhanced the THz signal using a $\chi^{(2)}$ inversion structure that was fabricated by the face-to-face bonding of two epitaxial (113)B wafers.[24] However, it was difficult to achieve an equivalent optical thickness of two cavity layers because they were grown on two GaAs substrates separately. In addition, much time and effort are required to completely remove one of the substrates from the bonded wafer for device processing. Therefore, sublattice reversal, which results in $\chi^{(2)}$ inversion without wafer bonding, is expected to be an alternative and more versatile growth technique for THz devices. Kondo and colleagues reported sublattice reversal in a GaAs/Ge/GaAs system on low-index (001) or (111) GaAs substrates.[25,26] This novel growth technique has been applied to several nonlinear optical devices based on low-index GaAs substrates.[27–29] However, as far as we know, there has been no experimental study of sublattice reversal on high-index GaAs substrates reported to date.

Here, we investigated GaAs/Ge/GaAs heterostructures on high-index (113)B GaAs substrates grown by molecular beam epitaxy (MBE). Sublattice reversal in GaAs/Ge/GaAs was identified by comparing the mesa shape produced by anisotropic etching of the individual GaAs layers with that for reference substrates. In addition, the atomic arrangements were directly observed using energy-dispersive X-ray spectroscopy (EDX) in combination with scanning transmission electron microscopy (STEM; JEOL JEM-ARM200F operated at 200 kV).

Figure 1 illustrates the basic concept of sublattice reversal epitaxy on a (113)B GaAs substrate. The insertion of a thin intermediate layer of group-IV atoms (Ge) is expected to reverse the sublattice occupation from sublattice 1 to 2, i.e.,

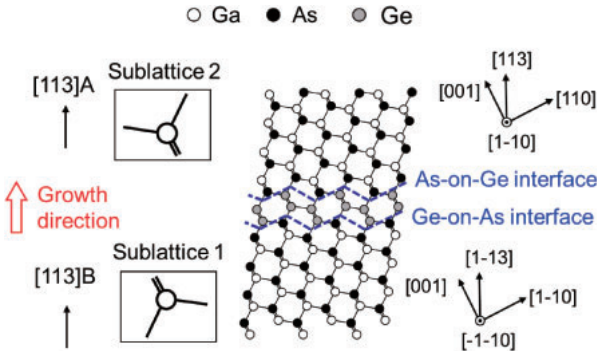

Fig. 1. Scheme of sublattice reversal in GaAs/Ge/GaAs heterostructures. Insertion of a thin intermediate layer of group-IV atoms (Ge) causes the sublattice occupation to change from sublattice 1 to 2, i.e., from (113)B to (113)A.

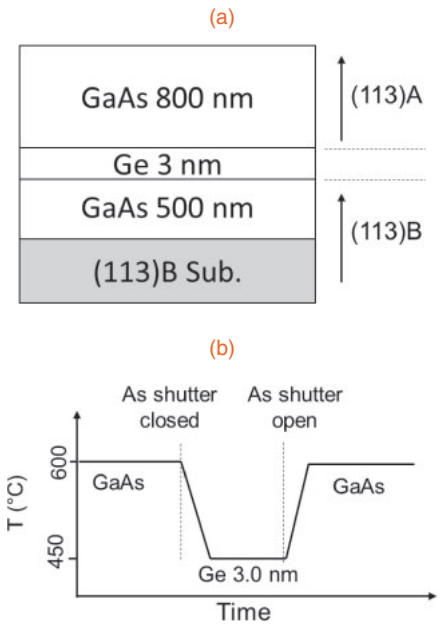

Fig. 2. (a) Epitaxial structure and (b) growth sequence for GaAs/Ge/GaAs heterostructure on (113)B GaAs.

from (113)B to (113)A. The epitaxial structure and growth sequence for the GaAs/Ge/GaAs heterostructures are shown in Figs. 2(a) and 2(b), respectively. After thermal cleaning of the substrate at 610 °C for 10 min, a 500-nm-thick GaAs buffer layer was grown at 600 °C. The As source shutter was then closed and the substrate temperature was decreased to 450 °C. A Ge layer with a nominal thickness of 3 nm was grown at 450 °C with the As source shutter closed. After the Ge growth, the As shutter was opened to establish an As prelayer and the substrate temperature was ramped up to 600 °C for the growth of an 800-nm-thick GaAs layer.

Orientation-dependent anisotropic etching[30] was employed to confirm the sublattice reversal. The etching rate is strongly dependent on the composition of the solution and on the GaAs crystal orientation, allowing the preferential etching of GaAs through photoresist masks. The epitaxial samples were patterned with a 10-μm-wide stripe photoresist running along the $[3\bar{3}\bar{2}]$ direction of the (113)B GaAs substrate. The upper 800-nm-thick GaAs layer and the 3-nm-thick Ge layer were etched sequentially using $H_2SO_4 : H_2O_2 = 1 : 10$ etchant at about 3 °C and $NH_4OH : H_2O_2 : H_2O = 2 : 1 : 100$ etchant at room temperature, respectively. The lower GaAs layer was then etched under the same conditions used for the upper GaAs layer. For comparison, reference (113)A and (113)B GaAs substrates without epitaxial layers were also etched with $H_2SO_4 : H_2O_2 = 1 : 10$ at about 3 °C.

Cross-sectional scanning electron microscopy (SEM) images of the anisotropic etching profile taken along the $[33\bar{2}]$ direction of the reference (113)A substrate and the $[3\bar{3}\bar{2}]$ direction of the reference (113)B substrate are shown in Figs. 3(a) and 3(b), respectively. It can be seen that the mesas have trapezoidal and inverse-trapezoidal shapes, respectively. Figure 3(c) shows a similar image for a GaAs/Ge/GaAs heterostructure grown on a (113)B GaAs substrate. The mesa shape for the lower GaAs layer is seen to be similar to that for the reference (113)B substrate, whereas that for the upper GaAs layer is similar to that for the reference (113)A substrate. These results confirm that sublattice reversal was achieved for the heterostructure grown on the (113)B GaAs substrate. This was also found to be the case when a Ge layer of 7 nm thickness was used. In contrast, sublattice reversal was not achieved for the heterostructure grown on the (113)A GaAs substrate, as shown in Fig. 3(d), where the mesas above and below the Ge layer both have inverse-trapezoidal shapes. The mechanism for sublattice reversal is discussed later; however, it is reasonable that the Ge surface was terminated by an As prelayer for both the (113)B and (113)A GaAs substrates. Figure 4 shows an atomic-resolution EDX elemental map of a GaAs/Ge/GaAs heterostructure grown on a (113)B GaAs substrate. The sublattice reversal from (113)B to (113)A can be directly observed from the atomic arrangements on the substrate and surface sides. Below the Ge layer, the left-side atoms in the Ga–As dumbbells are Ga atoms, while above the Ge layer, they are As atoms.

The mechanism of sublattice reversal in the GaAs/Ge/GaAs(100) system has been explained using an antiphase

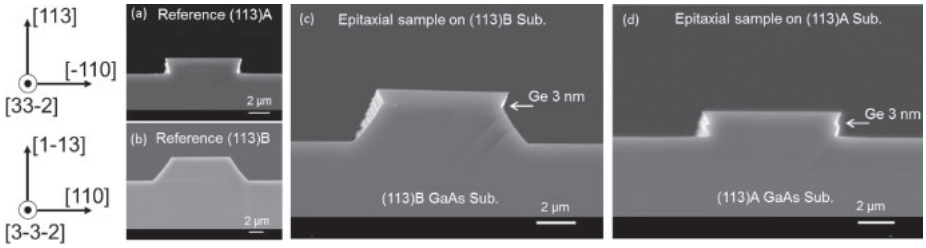

Fig. 3. Cross-sectional SEM images of etching profile obtained along $[33\bar{2}]$ direction. (a) Reference (113)A GaAs substrate. (b) Reference (113)B GaAs substrate. (c) Epitaxial sample on (113)B GaAs substrate. (d) Epitaxial sample on (113)A GaAs substrate.

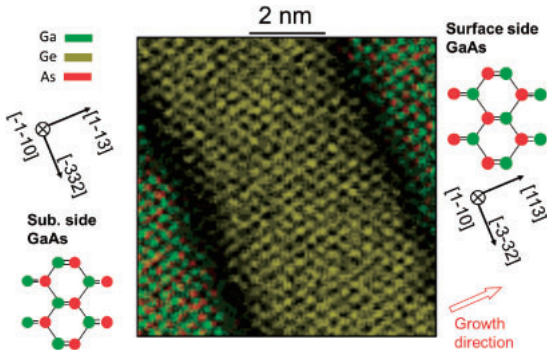

Fig. 4. Atomic-resolution EDX elemental map of epitaxial sample. Sublattice reversal is directly observed through the atomic arrangements.

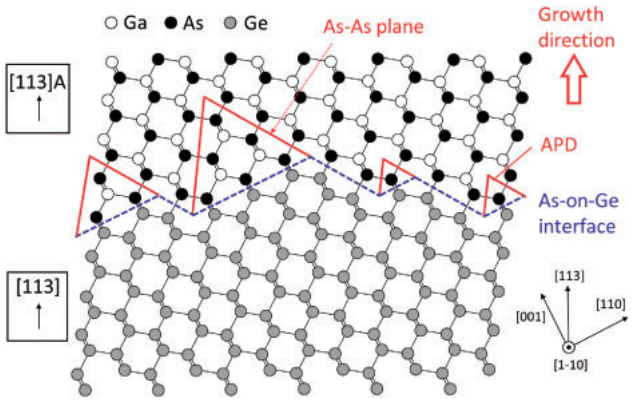

Fig. 5. Self-annihilation of APDs in GaAs epilayer grown on the Ge/GaAs layer formed on both (113)A and (113)B GaAs substrates.

domain (APD) self-annihilation model.[27] It is considered that this model is also valid for GaAs/Ge/GaAs on high-index GaAs substrates of the current study. Figure 5 shows a schematic illustration of the self-annihilation of APDs in GaAs grown on an As-terminated Ge layer. Antiphase boundaries (APBs), which are generated at step edges on the Ge surface, are composed of (111)B As–As bond planes. These APBs propagate on inclined (111) planes and encounter each other, resulting in their self-annihilation. The number of atomic height steps on (113) GaAs is larger than that on (001) GaAs. APBs are easily formed on these steps and APDs tend to become completely annihilated extremely fast. We did not find any evidence of APDs in the EDX map, which suggests that the APBs may be annihilated within the first few atomic layers. It is should be noted that APBs composed of As–As bond planes are always generated once the Ge layer is As-terminated, which is why sublattice reversal did not occur in the GaAs/Ge/GaAs heterostructure grown on the (113)A GaAs substrate, as shown in Fig. 3(d). Ebert et al. reported sublattice reversal on (001) GaAs slightly misoriented (by about 4°) towards ⟨111⟩A, using Ga-terminated Ge layers and migration-enhanced epitaxy (MEE).[31] Therefore, these techniques give rise to the possibility of the formation of Ga–Ga bond planes that result in the self-annihilation of (111)A planes and the realization of sublattice reversal on (113)A GaAs substrates.

In summary, sublattice reversal epitaxy on (113)B GaAs substrates is proposed as a versatile method of realizing $\chi^{(2)}$ inversion in THz devices. A GaAs/Ge/GaAs heterostructure was grown on a high-index (113)B GaAs substrate by MBE. Following anisotropic chemical etching of the heterostructure, sublattice reversal in GaAs/Ge/GaAs was confirmed by comparison of the mesa shape of the two GaAs layers with that of reference substrates. The mesa shape for the lower GaAs layer was similar to that for the reference (113)B substrate, whereas that for the upper GaAs layer was similar to that for the reference (113)A substrate. Furthermore, atomic-resolution EDX mapping was performed and sublattice reversal from (113)B to (113)A was directly observed through the atomic arrangements. APDs associated with As–As bond planes may be responsible for the observed sublattice reversal in the GaAs/Ge/GaAs system on the (113)B substrate.

Acknowledgments This work was supported in part by KAKENHI Grants-in-Aid (Nos. JP16H04351 and JP15K13956) from the Japan Society for the Promotion of Science (JSPS).

1) M. Tonouchi, Nat. Photonics **1**, 97 (2007).
2) R. A. Lewis, J. Phys. D **47**, 374001 (2014).
3) R. Köhler, A. Tredicucci, F. Beltram, H. E. Beere, E. H. Linfield, A. G. Davies, D. A. Ritchie, R. C. Iotti, and F. Rossi, Nature **417**, 156 (2002).
4) B. S. Williams, Nat. Photonics **1**, 517 (2007).
5) M. A. Belkin, J. A. Fan, S. Hormoz, F. Capasso, S. P. Khanna, M. Lachab, A. G. Davies, and E. H. Linfield, Opt. Express **16**, 3242 (2008).
6) M. Asada, S. Suzuki, and N. Kishimoto, Jpn. J. Appl. Phys. **47**, 4375 (2008).
7) S. Suzuki, M. Asada, A. Teranishi, H. Sugiyama, and H. Yokoyama, Appl. Phys. Lett. **97**, 242102 (2010).
8) S. Matsuura, M. Tani, and K. Sakai, Appl. Phys. Lett. **70**, 559 (1997).
9) S. H. Yang and M. Jarrahi, Appl. Phys. Lett. **107**, 131111 (2015).
10) K. Vijayraghavan, Y. Jiang, M. Jang, A. Jiang, K. Choutagunta, A. Vizbaras, F. Demmerle, G. Boehm, M. C. Amann, and M. A. Belkin, Nat. Commun. **4**, 2021 (2013).
11) K. Fujita, M. Hitaka, A. Ito, T. Edamura, M. Yamanishi, S. Jung, and M. A. Belkin, Appl. Phys. Lett. **106**, 251104 (2015).
12) N. Yamada, Y. Ichimura, S. Nakagawa, Y. Kaneko, T. Takeuchi, and N. Mikoshiba, Jpn. J. Appl. Phys. **35**, 2659 (1996).
13) T. Kitada, F. Tanaka, T. Takahashi, K. Morita, and T. Isu, Appl. Phys. Lett. **95**, 111106 (2009).
14) F. Tanaka, T. Takahashi, K. Morita, T. Kitada, and T. Isu, Jpn. J. Appl. Phys. **49**, 04DG01 (2010).
15) K. Morita, F. Tanaka, T. Takahashi, T. Kitada, and T. Isu, Appl. Phys. Express **3**, 072801 (2010).
16) F. Tanaka, T. Takimoto, K. Morita, T. Kitada, and T. Isu, Jpn. J. Appl. Phys. **50**, 04DG03 (2011).
17) K. Morita, S. Katoh, T. Takimoto, F. Tanaka, Y. Nakagawa, S. Saito, T. Kitada, and T. Isu, Appl. Phys. Express **4**, 102102 (2011).
18) S. Katoh, T. Takimoto, Y. Nakagawa, K. Morita, T. Kitada, and T. Isu, Jpn. J. Appl. Phys. **51**, 04DG05 (2012).
19) T. Kitada, S. Katoh, T. Takimoto, Y. Nakagawa, K. Morita, and T. Isu, IEEE Photonics J. **5**, 6500308 (2013).
20) T. Kitada, H. Ota, X. M. Lu, N. Kumagai, and T. Isu, Appl. Phys. Express **9**, 111201 (2016).
21) Y. Minami, H. Ota, X. M. Lu, N. Kumagai, T. Kitada, and T. Isu, Jpn. J. Appl. Phys. **56**, 04CH01 (2017).
22) T. Kitada, H. Ota, X. M. Lu, N. Kumagai, and T. Isu, IEICE Trans. Electron. **E100-C**, 171 (2017).
23) X. M. Lu, H. Ota, N. Kumagai, Y. Minami, T. Kitada, and T. Isu, J. Cryst. Growth **477**, 249 (2017).
24) T. Kitada, S. Katoh, T. Takimoto, Y. Nakagawa, K. Morita, and T. Isu, Appl. Phys. Lett. **102**, 251118 (2013).
25) T. Kondo, S. Koh, and R. Ito, Sci. Technol. Adv. Mater. **1**, 173 (2000).
26) S. Koh, T. Kondo, M. Ebihara, T. Ishiwada, H. Sawada, H. Ichinose, I. Shoji, and R. Ito, Jpn. J. Appl. Phys. **38**, L508 (1999).
27) S. Koh, T. Kondo, Y. Shiraki, and R. Ito, J. Cryst. Growth **227–228**, 183 (2001).
28) A. Grisard, E. Lallier, and B. Gérard, Opt. Mater. Express **2**, 1020 (2012).
29) J. Ota, W. Narita, I. Ohta, T. Matsushita, and T. Kondo, Jpn. J. Appl. Phys. **48**, 04C110 (2009).
30) M. Otsubo, T. Oda, H. Kumabe, and H. Miki, J. Electrochem. Soc. **123**, 676 (1976).
31) C. B. Ebert, L. A. Eyres, M. M. Fejer, and J. S. Harris, J. Cryst. Growth **201–202**, 187 (1999).